International Journal of Applied Pharmaceutics

ISSN- 0975-7058 Vol 16, Issue 6, 2024

Original Article

FABRICATION AND CHARACTERIZATION OF DISSOLVING MICRONEEDLE PATCH USING 3D PRINTED MASTER

SHRADDHA GUPTA, DHAKSHINAMOORTHY VASANTH*, AWANISH KUMAR

Department of Biotechnology, National Institute of Technology (NIT), Raipur, Chhattisgarh, India
***Corresponding author: Dhakshinamoorthy Vasanth; *Email: dvasanth.bt@nitrr.ac.in**

Received: 09 Aug 2024, Revised and Accepted: 10 Sep 2024

ABSTRACT

Objective: The purpose of this study was to fabricate a dissolving microneedle patch using a 3D-printed master and characterize it using various techniques.

Methods: Dissolving microneedle patches were developed using Computer-Aided Design (CAD) software and 3D printing. Polydimethylsiloxane (PDMS) reverse molds were cast from the 3D-printed masters and filled with a solution of 20% Chitosan Oligosaccharide (COS) and 20% Polyvinyl Alcohol (PVA). The patches were dried at room temperature and characterized using Scanning Electron Microscopy (SEM), Attenuated Total Reflectance-Fourier Transform Infrared Spectroscopy (ATR-FTIR), X-ray diffraction (XRD), Thermogravimetric Analysis (TGA), Differential Scanning Calorimetry (DSC), and in vitro skin penetration studies.

Results: Optical microscopy and SEM images showed the formation of a uniform microneedle. The peak at 1248 cm^{-1} in the ATR-FTIR spectrum indicates the formation of cross-links between certain PVA radical groups and COS. XRD revealed that both polymers blended well and showed partial crystallinity, with peaks at 2θ = 11.39°, 2θ = 20°, and 2θ = 41°. DSC and TGA analyses revealed that the blend could withstand high temperatures with good stability at temperatures up to 200 °C. *In vitro* skin penetration studies confirmed that microneedles could successfully penetrate the skin, indicating their potential for effective transdermal drug delivery.

Conclusion: This study demonstrated that COS/PVA dissolving microneedles fabricated using 3D printing and micro-molding have significant potential for transdermal drug delivery.

Keywords: Chitosan oligosaccharide, Polyvinyl alcohol, Dissolving microneedles, Characterization, Biopolymer

DOI: https://dx.doi.org/10.22159/ijap.2024v16i6.52314 Journal homepage: https://innovareacademics.in/journals/index.php/ijap

INTRODUCTION

Microneedles (MNs) are arrays of tiny needles that create small channels in the outermost layer of the skin, known as the stratum corneum [1, 2]. These minimally invasive devices have sufficient length to penetrate the permeability barrier while being sufficiently short and thin to prevent pain [3-5]. There are five different types of microneedle solids: solid [6], coated [7], hollow [8], hydrogel-forming [9], and dissolving [10, 11].

Dissolving microneedles are typically composed of biocompatible materials, such as sugars, proteins, or polymers, which dissolve or degrade upon insertion into the skin [12], as shown in fig. 1(a), releasing the payload of drugs or vaccines, as shown in fig. 1(b) [13, 14]. This requires precise handling and can be intimidating and painful, often resulting in distress for patients. Dissolving microneedles are alternatives to traditional needles that eliminate the need for sharp disposal [15]. Dissolving microneedles offers significant advantages over vaccines for drug delivery. They can deliver a wide range of therapeutics, including medications for chronic conditions such as diabetes and cardiovascular disease [16-18].

Various techniques have been employed in the fabrication of dissolving microneedles, such as micromolding, drawing lithography, droplet-born air blowing, and photopolymerization [19]. Micromolding is the most popular fabrication approach because of its high reproducibility. Another emerging technology that is currently in use is 3D printing. Advanced and intricate designs can be efficiently created with high accuracy over a short period [20-22]. 3D printing technology enables the efficient production of micromolds, resulting in time and cost savings [23, 24] because traditional techniques are labor-intensive and time-consuming.

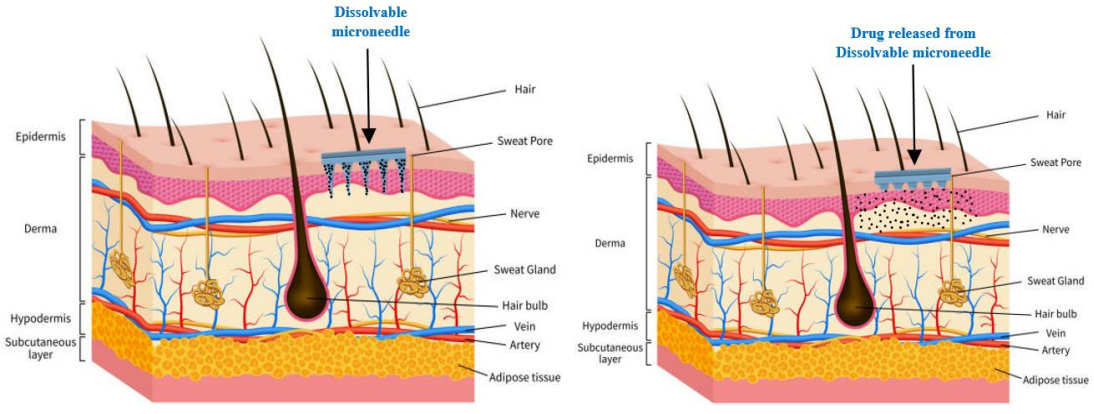

(a) **(b)**

Fig. 1: Dissolving microneedle process, (a) Microneedle inserted into the skin, (b) Microneedle dissolves, releasing the encapsulated medication [25, 26]

Although various materials and fabrication techniques have been explored, the combination of Chitosan Oligosaccharide (COS) and Polyvinyl Alcohol (PVA) in 3D-printed dissolving microneedles remains underexplored, particularly in terms of the mechanical strength and thermal stability. Considering these gaps, this study aimed to rigorously evaluate the fabrication of Chitosan Oligosaccharide/Polyvinyl Alcohol (COS/PVA) dissolving microneedles using 3D printed masters, with a focus on characterizing their mechanical strength. In this study, the microneedle master was printed using 3D printing. The microneedle master was then used as a template to construct a Polydimethylsiloxane (PDMS) reverse mold. Subsequently, a blend of COS and PVA was used as a polymeric material to fabricate dissolving microneedle patches, which were further characterized.

MATERIALS AND METHODS

Materials

(PDMS Sylgard 184 Silicone Elastomer Kit) was obtained from Dow Chemical Company (Midland, TX, USA). COS with a Molecular Weight>3000.00, and 90% deacetylation, was obtained from Sisco Research Laboratories Pvt. Ltd. (Taloja, Maharashtra, India). PVA with a molecular weight of 60,000-1,25,000 was obtained from HiMedia Laboratories Pvt. Ltd. (Thane, Maharashtra, India).

Method

Fabrication of dissolving microneedle

Fabrication of microneedle master using 3D printer

Dissolving microneedle arrays were designed using computer-aided design software (SolidWorks 2020, Dassault Systèmes SE, Vélizy-Villacoublay, France). The dissolving microneedles were designed as octagonal pyramids with a height of 1160 µm and a base width of 580 µm. The array comprised 324 microneedles arranged in an 18×18 pattern. The dimensions were selected based on previous studies [27] that demonstrated optimal skin penetration with minimal discomfort. Computer-Aided Design (CAD) drawings were converted to the STL file format and sliced using the Envision One RP software for 3D printing. The microneedle master was fabricated using a DLP-based 3D printer (EnVision D4K Pro; Envisiontec GmbH, Gladbeck, Germany) [28]. After fabrication, the mold was cured by exposure to 405 nm light for 3 min.

Fabrication of polydimethylsiloxane mold

The PDMS reverse mold was prepared by following the method of Tu and Chung [29] with slight modifications. The PDMS solution was prepared by mixing in a 10:1 ratio (10 parts base to one part curing agent). This mixture was thoroughly mixed and degassed to remove air bubbles. The PDMS solution was then poured onto the 3D printed microneedle master (18×18 array) and placed in a desiccator for 24-48 h to dry. After drying, the Polydimethylsiloxane (PDMS) reverse mold was carefully removed from the 3D-printed mold.

Fabrication of dissolving microneedle patch

To fabricate the dissolving microneedle patch, 20% (w/w) COS and 20% (w/w) PVA solutions were prepared separately. The prepared solutions were degassed and maintained at room temperature. The PVA solution was then added to the COS solution and mixed thoroughly to obtain a polymer solution. This polymer solution was poured into a PDMS reverse mold and spread evenly. Subsequently, it was maintained under vacuum to ensure that the needles were fully filled. The solution was then dried naturally at room temperature until microneedles were formed. Finally, the microneedles were removed from the reverse mold and stored in a desiccator until further use [30].

Physical and morphological characterization of dissolving microneedle patch

Microscopic evaluation

Optical microscope

The patch was initially examined using an Inverted Optical Microscope (Carl Zeiss Microscopy, Axio Vert A1 MAT: Carl Zeiss India Bangalore Pvt. Ltd., Bengaluru-560099) to assess the consistency of the needles throughout the patch [31].

Scanning electron microscopy

The surface morphology of the microneedle was observed by Scanning Electron Microscope (Carl Zeiss UHR FESEM Model GeminiSEM 500 KMAT; Carl Zeiss India Bangalore Pvt. Ltd., Bengaluru-560099). Prior to analysis, the dissolving microneedle (DMN) surface patches were coated with gold using a spray-coating machine (Quoram Sputter Coater Q150R S Plus) for 120 s [32].

Structural analysis

Attenuated total reflectance-fourier transform infrared spectroscopy analysis

To confirm the compatibility of the ingredients, complex formation, and confirmation of the functional groups, ATR-FTIR studies were conducted before and after patch fabrication. In this study, an ATR-FTIR Spectrophotometer (Thermo Fisher Scientific India Pvt. Ltd.,Thane, Maharashtra) was used to record the spectra of COS, PVA, and COS/PVA. Prior to the analysis, the instrument was calibrated by cleaning the ATR crystal with pure alcohol and performing a background scan to create a baseline. Following calibration, the sample was placed directly onto the ATR crystal to ensure optimal contact and enhance the strength of the signal. The analysis was performed using 24 scans in the 400–4000 cm^{-1} [33].

X-ray diffraction analysis

The amorphous and crystalline properties of COS, PVA, and COS/PVA were examined using powder-XRD with a Bruker D8 Advance A25 (Bruker India Pvt. Ltd. Bangaluru-560065). The samples were analyzed using monochromatized Cu Kα radiation at angles ranging from 5° to 80°. The analysis was conducted at a voltage of 40 kV and a current of 40 mA [34].

Thermal analysis

Thermogravimetric analysis

Weight loss in COS, PVA, and COS/PVA was measured using a TGA 8000 lab System (Perkin Elmer India Pvt. Ltd., Bangaluru-560102). A 5 mg sample was placed in the TGA pan loaded onto the balance mechanism inside the furnace. The samples were analyzed in a nitrogen atmosphere at a scanning rate of 10 °C/min within a temperature range of 0–900 °C [35].

Differential scanning calorimetry analysis

The thermal properties of COS, PVA, and COS/PVA were analyzed using DSC (Perkin Elmer India Pvt. Ltd. Bangaluru-560102). Five milligrams of the sample was placed in a DSC pan, and the sample was examined under a nitrogen atmosphere at a scanning rate of 10 °C/min, covering a temperature range of 0–400 °C [36].

In vitro skin penetration study

Parafilm® M, an artificial skin simulator, was used to measure the penetration depth of the dissolving microneedles. The film was folded eight times before the microneedle was placed on top of the first layer. The array was perforated into layers using thumb pressure to ease its placement in the film. The microneedle was examined under a digital microscope after insertion to observe morphological changes and tip bending. A digital microscope was used to examine the Parafilm ® M layer and to count the number of holes created by the microneedle [37].

RESULTS AND DISCUSSION

Microscopic evaluation

Optical microscope

Following the fabrication of the microneedles, an initial assessment was performed by observing the microneedle patch using an optical microscope (fig. 2). This investigation yielded comprehensive insights into the morphology of the microneedles. By evaluating the consistency, acuity of the tips, and overall architecture, we verified

that the microneedles were fabricated accurately and appropriately for subsequent analyses. This initial optical assessment ensures that the microneedles are consistently formed and free of defects before proceeding to more detailed analyses, such as SEM.

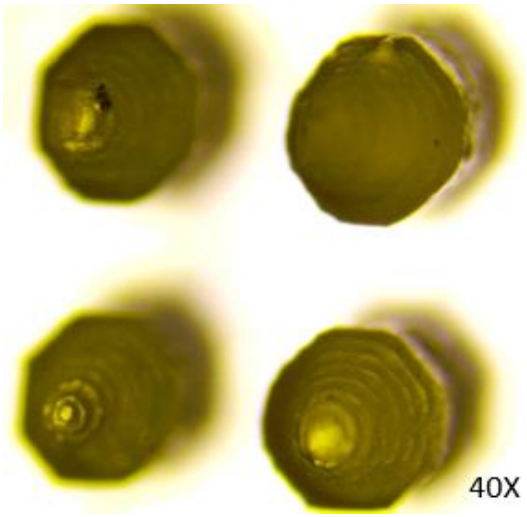

Fig. 2: Digital microscope image of COS/PVA microneedle patch, highlighting the uniformity and alignment of microneedles across the patch surface

Scanning electron microscopy analysis

The SEM image (fig. 3) shows a detailed view of the microneedles from the dissolving microneedle patch. The microneedles exhibited a well-defined octagonal pyramid shape with distinct layers, reflecting the precision of the layering process used in their fabrication. Uniformity is evident across the different microneedles, which is crucial for consistent performance in practical applications. The tips of the microneedles were pointed out, indicating the successful creation of sharp tips, which are essential for effective skin penetration. The surface of the microneedles showed a textured pattern, likely a result of the layering or 3D printing process, which could potentially enhance the dissolution process once the microneedles are inserted into the skin. In addition, the absence of visible defects, cracks, and irregularities confirmed the structural integrity and robustness of the microneedles, ensuring that they did not break during skin insertion. Overall, the SEM images verified that the microneedles were well fabricated with the desired morphological characteristics, making them suitable for further functional testing and potential applications in transdermal drug delivery. The observed uniformity and sharpness of the microneedles align with the findings of Faisal [38], who also utilized 3D printing for microneedle fabrication.

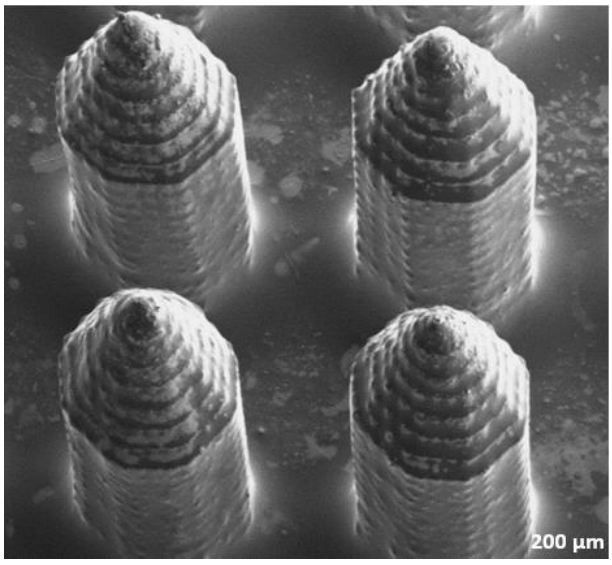

Fig. 3: SEM image of COS/PVA dissolving microneedles, showing well-defined tips essential for skin penetration

Structural analysis

Attenuated total reflectance-fourier transform infrared spectroscopy analysis

The ATR-FTIR spectra (fig. 4) of COS, PVA, and their blends in dissolving microneedles were analyzed to understand their molecular structures and interactions. The COS spectrum displayed peaks indicative of its polysaccharide structure, including amide I (C=O vibration mode) at 1629 cm^{-1}, amide II (N–H bending vibration mode) at 1517 cm^{-1}, and amide III at 1380 cm^{-1} [39], whereas the peak at 1079 cm^{-1} confirmed the presence of chitosan. Peak in the 3650-3250 cm^{-1} range indicates hydrogen bonding and C–O–C bond stretching.

Hydroxyls are expected to display frequencies in the 1600–1300 cm-1, 1200–1000 cm-1, and 800–600 cm-1 ranges [40]. The PVA spectrum exhibited a strong O—H bond at 3439 cm^{-1}, CH_2 asymmetric stretching at 2928 cm^{-1}, and water absorption at 1633 cm^{-1}. Other significant peaks included C—O stretching at 1328 cm^{-1}, stretching of C—O and bending of OH groups at 1083 $cm^{-1,}$ and C—C stretching at 822 cm^{-1}. Saadiah *et al.* [41] reported the same characteristic peaks for PVA. In the COS/PVA blend spectrum, notable peaks included the N-H group at 3308 cm^{-1}, CH_2 asymmetric vibration at 2942 cm^{-1}, and C=O bonds at 1715 and 1085 cm^{-1}. The peak at 1248 cm^{-1} in the infrared spectrum indicates the formation of cross-links between certain PVA radical groups and COS. Crosslinking is crucial because it enhances the stability of the polymer structure, making it more robust and less likely to degrade rapidly. This stability is particularly important in drug delivery systems, in which a stable matrix ensures that the drug is released in a controlled manner over a longer period [42]. Mondal and He *et al.* [43, 44] confirmed that strong bonds within the polymer matrix ensure that the drug is released gradually, which is beneficial for maintaining consistent therapeutic levels and preventing rapid drug release.

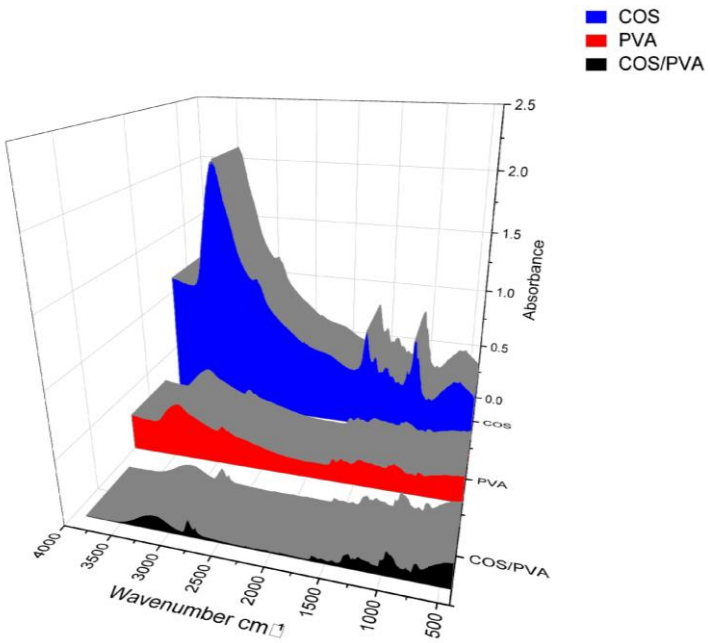

Fig. 4: ATR-FTIR spectra of COS, PVA, and COS/PVA dissolving microneedle, illustrating characteristic peaks and molecular interactions between the components

X-ray diffraction analysis

XRD analysis was conducted on both the raw materials and dissolving microneedle samples, as depicted in fig. 5. The XRD pattern of COS showed a broad peak at approximately 24.62°, indicating its amorphous nature and the lack of sharp peaks suggests the absence of a well-defined crystalline structure [45]. In contrast, the XRD pattern of PVA exhibited sharp peaks at 20° and 41°, reflecting its semi-crystalline nature, with the peak at 20° being particularly intense [46-50]. PVA semicrystalline structure of PVA is maintained by intermolecular and intramolecular hydrogen bonding [51]. From the XRD spectra of PVA and COS, it can be inferred that PVA exhibits a greater level of crystallinity than COS. The XRD pattern of the COS/PVA dissolving microneedles showed peaks at 2θ = 11.39°, 2θ = 20°, and 2θ = 41°. The first two peaks are smaller than the peak at 2θ = 41°, which is attributed to the blending of COS with PVA. The crystallinity was reduced, probably owing to the hydrogen bond interactions between COS and PVA [52].

XRD analysis revealed that COS was amorphous, whereas PVA was semicrystalline. The COS/PVA blend combines these properties, retaining the crystallinity of PVA and introducing new crystalline interactions. Bach [53] stated that higher crystallinity in the polymer matrix may lead to slower drug release rates, while lower crystallinity can enhance drug solubility and release. Thus, the COS/PVA blend exhibited lower crystallinity, which in turn enhanced solubility and facilitated more efficient drug release.

Thermal analysis

Differential scanning calorimetry analysis

Fig. 6 shows a DSC graph of the COS, revealing multiple thermal transitions. Initially, an endothermic peak at approximately 75 °C indicated the loss of loosely bound water. This was followed by an exothermic peak at approximately 130 °C, suggesting crystallization or structural reorganization of the COS material. A significant endothermic trough at approximately 200 °C indicates the primary melting point or the onset of thermal degradation. Additionally, a minor endothermic event between 250 and 300 °C suggests further decomposition or secondary transitions. For PVA, the broad endothermic peak up to 100 °C represents moisture loss and polymer relaxation. The endothermic peak at approximately 100–150 °C was due to the removal of bound water. The exothermic peak at 200 °C indicates crystallization, whereas the significant endothermic trough at approximately 230 °C indicates the melting point or onset of thermal degradation. A minor endothermic activity above 250 °C suggests further decomposition [54-56]. The DSC thermogram of the COS/PVA blend showed a gradual decrease in heat flow from 50 to 150 °C, which can be attributed to the evaporation of residual moisture or the release of bound water within the blend. This dehydration step is crucial because it indicates the presence of water molecules in the polymer matrix, which may affect the thermal properties of the blend. The DSC curve exhibited an endothermic peak at approximately 217 °C. This peak likely corresponds to the melting of the crystalline regions of COS or relaxation of the amorphous regions within the polymer blend. The energy absorbed during this phase transition suggests that PVA component in the blend underwent a significant structural change. A more pronounced endothermic peak was observed at approximately 250 °C. This peak indicates another major thermal transition, which could be associated with the thermal degradation or melting of the PVA component. The distinct nature of this peak suggests considerable energy absorption, reflecting the thermal stability and phase behavior of COS within the blend. After the second peak, the heat flow decreased, indicating ongoing thermal degradation processes within the material. This thermal degradation can be linked to the breakdown of the polymer chains and the formation of volatile degradation products.

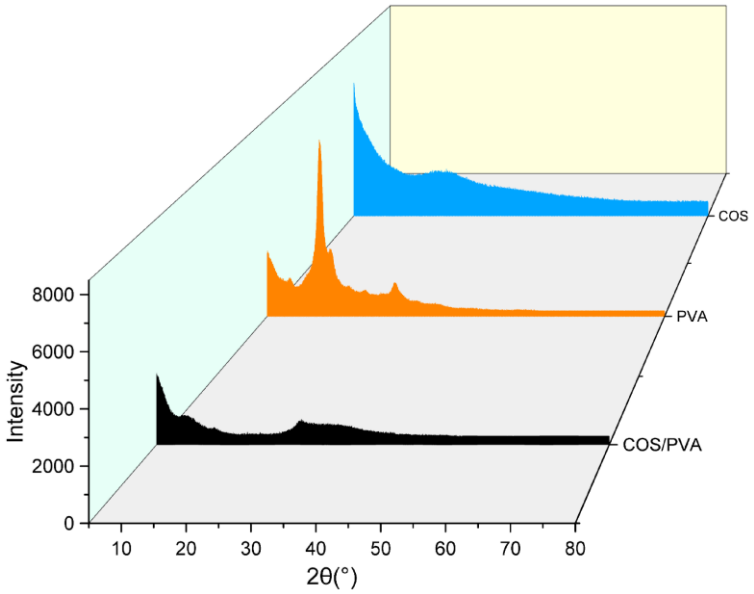

Fig. 5: XRD patterns of COS, PVA, and COS/PVA dissolving microneedle, highlighting crystalline interactions and structural changes in the composite material

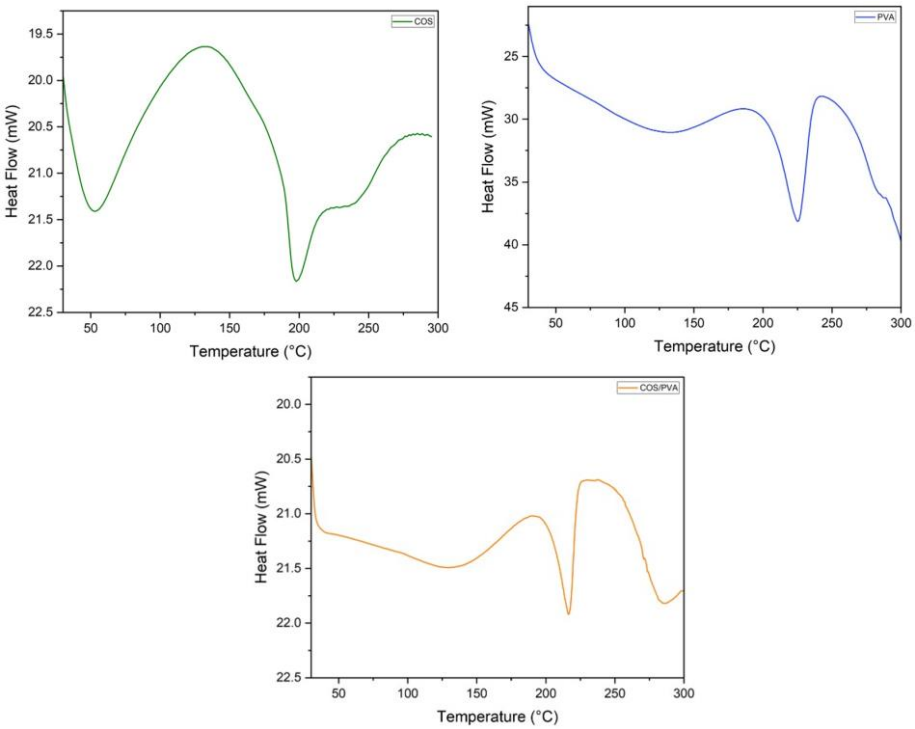

Fig. 6: DSC thermogram of COS, PVA, and COS/PVA dissolving microneedle, depicting thermal transitions and indicating the compatibility and stability of the blended materials

Thermogravimetric analysis

The thermal stabilities of the raw materials and microneedles were evaluated using TGA. The thermogram (fig. 7) of COS shows primary thermal degradation between 100-300 °C, with significant weight loss indicating molecular breakdown. Similar results were reported by Yue *et al.* and Appunni *et al.* [39, 57]. Beyond this range, the degradation slowed, leaving residual char that gradually decomposed up to 800 °C. Conversely, the thermogram of PVA (fig. 6) indicates stability up to 200 °C, followed by significant degradation between 300-450 °C, with near-total degradation at 600 °C, leaving minimal residue. This thermal profile highlights PVA suitability for high-temperature processing for industrial and biomedical applications. The thermogram of the COS/PVA blend showed a combined thermal degradation profile, starting with stability up to 200 °C, followed by significant degradation from to 200-450 °C, and continued decomposition up to 600 °C. The near-total degradation at 800 °C demonstrated that the blend efficiently decomposed at high temperatures, leaving a minimal residual weight.

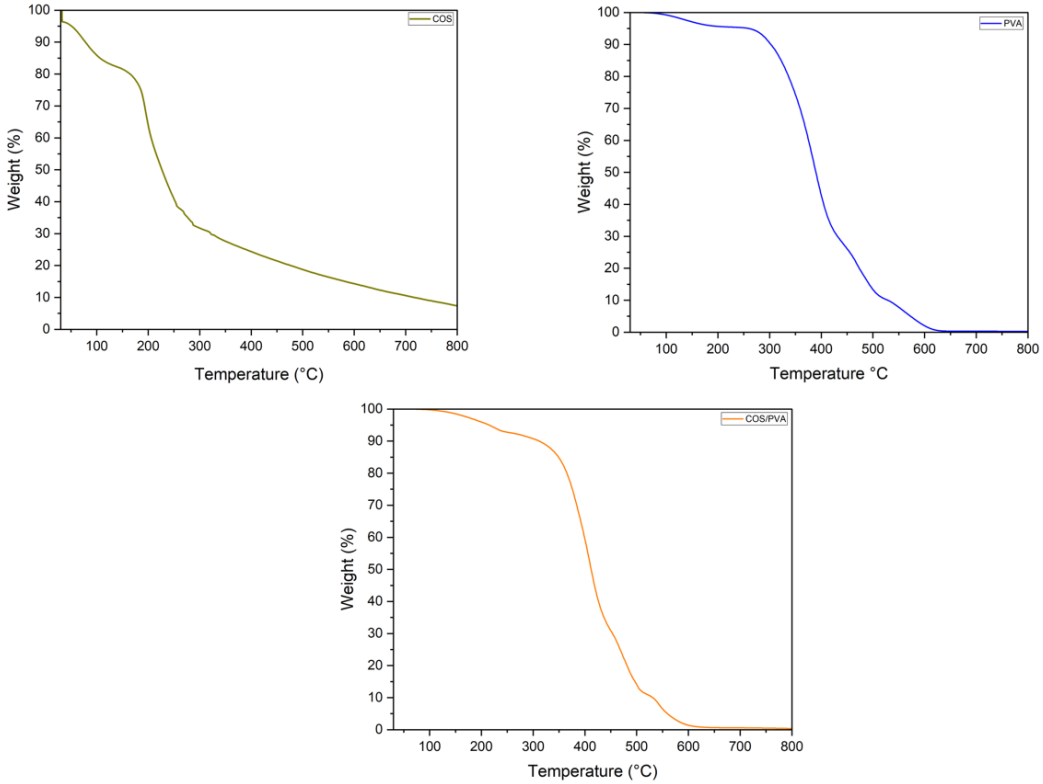

Fig. 7: TGA thermogram of COS, PVA, and COS/PVA dissolving microneedle, demonstrating thermal degradation profiles and stability of the individual and composite materials

In practical terms, the thermal stability observed in the DSC and TGA analyses of the COS/PVA microneedles indicates that they can be stored for extended periods without requiring strict temperature control, thereby reducing storage and distribution costs and complexity. Furthermore, their ability to withstand higher temperatures before degradation makes these microneedles suitable for use in a broader range of climates and healthcare settings, thereby ensuring their reliability and effectiveness in the delivery of therapeutic agents.

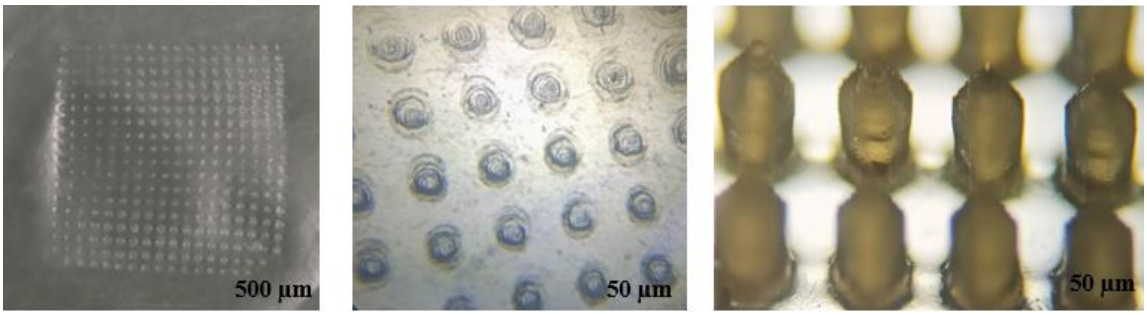

(a) **(b)** **(c)**

Fig. 8: (a) Photograph showing parafilm with fully inserted dissolving microneedle, providing a comprehensive view of insertion depth; (b) Microscopic image of parafilm detailing the microneedle insertion sites; (c) Photograph of the microneedle post-insertion, illustrating structural integrity after application

In vitro skin insertion study

The parafilm technique was used to assess the insertion efficacy of the microneedles in the simulated skin. Fig. 8 (a) and (b) demonstrate that all 324 needles in the 18×18 array successfully penetrated six layers of parafilm, as observed under a microscope. This confirmed the effective penetration capability of COS/PVA dissolving microneedles. Detailed microscopic analysis (fig. 8 (c)) further revealed that the needles maintained their structural integrity with no deformation and remained intact from the tip to the base, indicating their robustness and suitability for consistent skin penetration.

CONCLUSION

This study explored the fabrication and characterization of Dissolving Microneedles (DMNs) using a blend of COS and PVA and utilizing 3D printing technology for precise mold preparation. The microneedles demonstrated exceptional structural integrity, with optical and scanning electron microscopy confirming a well-formed, defect-free octagonal pyramid shape. ATR-FTIR analysis indicated successful cross-linking between COS and PVA, which enhanced the mechanical stability of the microneedles. Thermal analysis through DSC and TGA revealed key thermal transitions and degradation profiles, confirming the suitability of the material for biomedical

applications. Specifically, DSC identified moisture loss, crystallization, and thermal degradation, whereas TGA showed combined degradation profiles for the COS/PVA blends. *In vitro* penetration studies validated the ability of microneedles to effectively penetrate artificial skin layers, demonstrating their practical applicability in transdermal drug delivery. The results from the current study confirm the potential of using 3D printing technology in the fabrication of dissolving microneedles to achieve the desired design and mechanical and thermal stabilities. Thus, future research could explore the optimization of microneedle formulations with different polymer blends or evaluate their *in vivo* performance in animal models, further advancing their potential as viable alternatives to traditional hypodermic needles for drug delivery.

ACKNOWLEDGEMENT

The authors are thankful to the National Institute of Technology Raipur (CG), India, for their support.

FUNDING

The authors declare no conflicts of interest.

ABBREVIATION

COS-Chitosan Oligosaccharide, PVA-Polyvinyl Alcohol, PDMS – Polydimethylsiloxane, SEM-Scanning Electron Microscopy, ATR-FTIR-Attenuated Total Reflectance-Fourier Transform Infrared, XRD-X-Ray Diffraction, DSC-Differential Scanning Calorimetry, TGA-Thermogravimetric Analysis, DMN – Dissolving Microneedle.

AUTHORS CONTRIBUTIONS

Shraddha Gupta: writing-original draft, methodology, Conceptualization; Dhakshinamoorthy Vasanth: Writing, review and editing, supervision, conceptualization. Awanish Kumar: Writing, review and editing, supervision, conceptualization.

CONFLICT OF INTERESTS

The authors declare that they have no conflicts of interest.

REFERENCES

1. Sekar L, Seenivasan R, Reddy MV, Varma KD, Ahmed SS, Pachiyappan JK. Advancements in microneedle technology: comprehensive insights into versatile drug delivery mechanisms. Int J App Pharm. 2024;16(2):1-11. doi: 10.22159/ijap.2024v16i2.49564.
2. Ita K. Transdermal delivery of drugs with microneedles potential and challenges. Pharmaceutics. 2015;7(3):90-105. doi: 10.3390/pharmaceutics7030090, PMID 26131647.
3. Manoj VR, Manoj H. Review on transdermal microneedle-based drug delivery. Asian J Pharm Clin Res. 2019;12(1):18-29. doi: 10.22159/ajpcr.2019.v12i1.27434.
4. Gill HS, Denson DD, Burris BA, Prausnitz MR. Effect of microneedle design on pain in human volunteers. Clin J Pain. 2008;24(7):585-94. doi: 10.1097/AJP.0b013e31816778f9, PMID 18716497.
5. Chen W, Wang C, Yan L, Huang L, Zhu X, Chen B. Improved polyvinylpyrrolidone microneedle arrays with non-stoichiometric cyclodextrin. J Mater Chem B. 2014;2(12):1699-705. doi: 10.1039/c3tb21698e, PMID 32261399.
6. Hoang MT, Ita KB, Bair DA. Solid microneedles for transdermal delivery of amantadine hydrochloride and pramipexole dihydrochloride. Pharmaceutics. 2015;7(4):379-96. doi: 10.3390/pharmaceutics7040379, PMID 26426039.
7. Chong RH, Gonzalez Gonzalez E, Lara MF, Speaker TJ, Contag CH, Kaspar RL. Gene silencing following sirna delivery to skin via coated steel microneedles: *in vitro* and *in vivo* proof of concept. J Control Release. 2013;166(3):211-9. doi: 10.1016/j.jconrel.2012.12.030, PMID 23313112.
8. Jun H, Han MR, Kang NG, Park JH, Park JH. Use of hollow microneedles for targeted delivery of phenylephrine to treat fecal incontinence. J Control Release. 2015 Jun 10;207:1-6. doi: 10.1016/j.jconrel.2015.03.031, PMID 25828366.
9. Caffarel Salvador E, Tuan Mahmood TM, McElnay JC, McCarthy HO, Mooney K, Woolfson AD. Potential of hydrogel-forming and dissolving microneedles for use in paediatric populations. Int J Pharm. 2015;489(1-2):158-69. doi: 10.1016/j.ijpharm.2015.04.076, PMID 25940042.
10. Cole G, McCaffrey J, Ali AA, McBride JW, McCrudden CM, Vincente Perez EM. Dissolving microneedles for DNA vaccination: improving functionality via polymer characterization and Rala complexation. Hum Vaccin Immunother. 2017;13(1):50-62. doi: 10.1080/21645515.2016.1248008, PMID 27846370.
11. Lee JW, Park JH, Prausnitz MR. Dissolving microneedles for transdermal drug delivery. Biomaterials. 2008;29(13):2113-24. doi: 10.1016/j.biomaterials.2007.12.048.
12. Tiwari A, Sharma S, Soni PK, Paswan SK. Fabrication and development of dissolving microneedle patch of butorphanol tartrate. Int J App Pharm. 2023;15(3):261-71, doi: 10.22159/ijap.2023v15i3.47411.
13. Rajabi M, Roxhed N, Shafagh RZ, Haraldson T, Fischer AC, Wijngaart WV. Flexible and stretchable microneedle patches with integrated rigid stainless steel microneedles for transdermal biointerfacing. PLOS ONE. 2016;11(12):e0166330. doi: 10.1371/journal.pone.0166330, PMID 27935976.
14. Kim YC, Park JH, Prausnitz MR. Microneedles for drug and vaccine delivery. Adv Drug Deliv Rev. 2012;64(14):1547-68. doi: 10.1016/j.addr.2012.04.005, PMID 22575858.
15. Qiu Y, LI C, Zhang S, Yang G, HE M, Gao Y. Systemic delivery of artemether by dissolving microneedles. Int J Pharm. 2016;508(1-2):1-9. doi: 10.1016/j.ijpharm.2016.05.006, PMID 27150946.
16. Wang Q, Yao G, Dong P, Gong Z, LI G, Zhang K. Investigation on fabrication process of dissolving microneedle arrays to improve effective needle drug distribution. Eur J Pharm Sci. 2015;66:148-56. doi: 10.1016/j.ejps.2014.09.011, PMID 25446513.
17. Yao G, Quan G, Lin S, Peng T, Wang Q, Ran H. Novel dissolving microneedles for enhanced transdermal delivery of levonorgestrel: *in vitro* and *in vivo* characterization. Int J Pharm. 2017;534(1-2):378-86. doi: 10.1016/j.ijpharm.2017.10.035, PMID 29051119.
18. Zhang Q, XU C, Lin S, Zhou H, Yao G, Liu H. Synergistic immunoreaction of acupuncture-like dissolving microneedles containing thymopentin at acupoints in immune suppressed rats. Acta Pharm Sin B. 2018;8(3):449-57. doi: 10.1016/j.apsb.2017.12.006.
19. Ita K. Dissolving microneedles for transdermal drug delivery: advances and challenges. Biomed Pharmacother. 2017;93:1116-27. doi: 10.1016/j.biopha.2017.07.019, PMID 28738520.
20. Gou M, Qu X, Zhu W, Xiang M, Yang J, Zhang K, et al. Bio-inspired detoxification using 3d-printed hydrogel nanocomposites. Nat Commun. 2014;5(1):3774. doi: 10.1038/ncomms4774, PMID 24805923.
21. Zhang J, Chen Y, Huang Y, WU W, Deng X, Liu H. A 3d-printed self-adhesive bandage with drug release for peripheral nerve repair. Adv Sci (Weinh). 2020;7(23):2002601. doi: 10.1002/advs.202002601, PMID 33304766.
22. Kuril A, Ambekar A, Nimase B, Giri P, Nikam P, Desai H. Exploring the potential of 3d printing in pharmaceutical development. Int J Curr Pharm Sci. 2023;15(6):31-42. doi: 10.22159/ijcpr.2023v15i6.3085.
23. Krieger KJ, Bertollo N, Dangol M, Sheridan JT, Lowery MM, O'Cearbhaill ED. Simple and customizable method for fabrication of high-aspect-ratio microneedle molds using low-cost 3d printing. Microsyst Nanoeng. 2019;5(1):31645996. doi: 10.1038/s41378-019-0088-8.
24. Lee S, Wajahat M, Kim JH, Pyo J, Chang WS, Cho SH. Electroless deposition-assisted 3d printing of micro circuitries for structural electronics. ACS Appl Mater Interfaces. 2019;11(7):7123-30. doi: 10.1021/acsami.8b18199, PMID 30681321.
25. Istock, Getty images. Canada. Available from. https://www.istockphoto.com/search/2/image-ffilm?family=creativeandphrase=skin%20anatomy [Last accessed on 08 Oct 2024]

26. BioRender. Biorender. Canada. Available from: https://app.com/illustrations/65951fe379282c9642903da2. [Last accessed on 08 Oct 2024]
27. HE J, Zhang Z, Zheng X, LI L, QI J, WU W. Design and evaluation of dissolving microneedles for enhanced dermal delivery of propranolol hydrochloride. Pharmaceutics. 2021;13(4):33921712. doi: 10.3390/pharmaceutics13040579, PMID 33921712.
28. Johnson AR, Procopio AT. Low cost additive manufacturing of microneedle masters. 3D Print Med. 2019;5(1):2. doi: 10.1186/s41205-019-0039-x, PMID 30715677.
29. TU KT, Chung CK. Rapid prototyping of biodegradable microneedle arrays by integrating CO_2 laser processing and polymer molding. J Micromech Microeng. 2016;26(6):065015. doi: 10.1088/0960-1317/26/6/065015.
30. Dillon C, Hughes H, O'Reilly NJ, McLoughlin P. Formulation and characterisation of dissolving microneedles for the transdermal delivery of therapeutic peptides. Int J Pharm. 2017;526(1-2):125-36. doi: 10.1016/j.ijpharm.2017.04.066, PMID: 28461268.
31. Nguyen HX, Bozorg BD, Kim Y, Wieber A, Birk G, Lubda D. Poly (vinyl alcohol) microneedles: fabrication characterization and application for transdermal drug delivery of doxorubicin. Eur J Pharm Biopharm. 2018;129:88-103. doi: 10.1016/j.ejpb.2018.05.017, PMID 29800617.
32. Monkare J, Reza Nejadnik MR, Baccouche K, Romeijn S, Jiskoot W, Bouwstra JA. Igg-loaded hyaluronan-based dissolving microneedles for intradermal protein delivery. J Control Release. 2015;218:53-62. doi: 10.1016/j.jconrel.2015.10.002, PMID 26437262.
33. Bhadale RS, Londhe VY. Inclusion complexed iloperidone loaded dissolving microneedles: characterization *in vitro* study and dermatopharmacokinetics. J Drug Deliv Sci Technol. 2022 Feb;68:103063. doi: 10.1016/j.jddst.2021.103063.
34. Gugulothu D, Choudhary SK. Design and *in vitro* evaluation of floating drug delivery system of glipizide using combination of natural mucilages and synthetic polymers. Int J Pharm Pharm Sci. 2021;13:40-8. doi: 10.22159/ijpps.2021v13i7.41644.
35. Pervez S, Nasir F, Hidayatullah T, Khattak MA, Alasmari F, Zainab SR. Transdermal delivery of glimepiride: a novel approach using nanomicelle embedded microneedles. Pharmaceutics. 2023;15(8):37631233. doi: 10.3390/pharmaceutics15082019, PMID 37631233.
36. Farooqui P, Gude R. Formulation development and optimisation of fast dissolving buccal films loaded glimepiride solid dispersion with enhanced dissolution profile using central composite design. Int J Pharm Pharm Sci. 2023;15(6):35-54. doi: 10.22159/ijpps.2023v15i6.47992.
37. Scypinski S. Editorial: 2021 the year of returning to normalcy hopefully. J Pharm Innov. 2021;16(1):1. doi: 10.1007/s12247-021-09545-6, PMID 33680214.
38. Aldawood FK, Parupelli SK, Andar A, Desai S. 3D printing of biodegradable polymeric microneedles for transdermal drug delivery applications. Pharmaceutics. 2024;16(2):237. doi: 10.3390/pharmaceutics16020237, PMID 38399291.
39. Yue L, Zheng M, Wang M, Khan IM, Wang B, MA X. A general strategy to synthesis chitosan oligosaccharide-O-terpineol derivatives with antibacterial properties. Carbohydr Res. 2021;503:108315. doi: 10.1016/j.carres.2021.108315, PMID 33865180.
40. Yue L, LI J, Chen W, Liu X, Jiang Q, Xia W. Geraniol grafted chitosan oligosaccharide as a potential antibacterial agent. Carbohydr Polym. 2017;176:356-64. doi: 10.1016/j.carbpol.2017.07.043.
41. Saadiah MA, Zhang D, Nagao Y, Muzakir SK, Samsudin AS. Reducing crystallinity on thin film-based Cmc/Pva hybrid polymer for application as a host in polymer electrolytes. J Non-Crystal Solids. 2019;511:201-11. doi: 10.1016/j.jnoncrysol.2018.11.032.
42. Tiwari G, Tiwari R, Sriwastawa B, Bhati L, Pandey S, Pandey P. Drug delivery systems: an updated review. Int J Pharm Investig. 2012;2(1):2-11. doi: 10.4103/2230-973X.96920, PMID 23071954.
43. Mondal N. The role of matrix tablet in drug delivery system. Int J App Pharm. 2018;10(1):1-6. doi: 10.22159//ijap.2018v10i1.21935.
44. HE MC, Chen BZ, Ashfaq M, Guo XD. Assessment of mechanical stability of rapidly separating microneedles for transdermal drug delivery. Drug Deliv Transl Res. 2018;8(5):1034-42. doi: 10.1007/s13346-018-0547-z, PMID 29845379.
45. Mourya VK, Inamdar NN, Choudhari YM. Chitooligosaccharides: synthesis characterization and applications. Polym Sci Ser A. 2011;53(7):583-612. doi: 10.1134/S0965545X11070066.
46. Jia X, LI Y, Zhang B, Cheng Q, Zhang S. Preparation of poly(vinyl alcohol)/kaolinite nanocomposites via in situ polymerization. Mater Res Bull. 2008;43(3):611-7. doi: 10.1016/j.materresbull.2007.04.008.
47. Gupta S, Pramanik AK, Kailath A, Mishra T, Guha A, Nayar S. Composition-dependent structural modulations in transparent poly(vinyl alcohol) hydrogels. Colloids Surf B Biointerfaces. 2009;74(1):186-90. doi: 10.1016/j.colsurfb.2009.07.015, PMID: 19700267.
48. Pandele AM, Ionita M, Crica L, Dinescu S, Costache M, Iovu H. Synthesis characterization and *in vitro* studies of graphene oxide/chitosan polyvinyl alcohol films. Carbohydr Polym. 2014;102:813-20. doi: 10.1016/j.carbpol.2013.10.085, PMID 24507351.
49. Aziz SB. Modifying poly(vinyl alcohol) (pva) from insulator to small bandgap polymer: a novel approach for organic solar cells and optoelectronic devices. J Electron Mater. 2016;45(1):736-45. doi: 10.1007/s11664-015-4191-9.
50. Abdullah OG, Saleem SA. Effect of copper sulfide nanoparticles on the optical and electrical behavior of poly(vinyl alcohol) films. J Electron Mater. 2016;45(11):5910-20. doi: 10.1007/s11664-016-4797-6.
51. Abdullah OG, Aziz SB, Rasheed MA. Structural and optical characterization of PVA:KMnO 4 based solid polymer electrolyte. Results Phys. 2016;6:1103-8. doi: 10.1016/j.rinp.2016.11.050.
52. Lee HW, Karim MR, Park JH, Ghim HD, Choi JH, Kim K. Poly(vinyl alcohol)/chitosan oligosaccharide blend submicrometer fibers prepared from aqueous solutions by the electrospinning method. J Appl Polym Sci. 2009;111(1):132-40. doi: 10.1002/app.29033.
53. Bach F, Staufenbiel S, Bodmeier R. Implications of changes in physical state of drugs in poly(Lactide-Co-Glycolide) matrices upon exposure to moisture and release medium. J Drug Deliv Sci Technol. 2023;80:104115. doi: 10.1016/j.jddst.2022.104115.
54. Ren M, Frimmel FH, Abbt Braun G. Multi cycle photocatalytic degradation of bezafibrate by a cast polyvinyl alcohol/titanium dioxide (Pva/Tio2) hybrid film. J Mol Cat A Chem. 2015 May 1;400:42-8. doi: 10.1016/j.molcata.2015.02.004.
55. Zor M, Sen F, Candan Z, Ivanov E, Batakliev T, Georgiev V. Preparation and characterization of polyvinyl alcohol (Pva)/carbonized waste rubber biocomposite films. Polymers. 2024;16(8):38674970. doi: 10.3390/polym16081050, PMID 38674970.
56. Abitbol T, Johnstone T, Quinn TM, Gray DG. Reinforcement with cellulose nanocrystals of poly(vinyl alcohol) hydrogels prepared by cyclic freezing and thawing. Soft Matter. 2011;7(6):2373-9. doi: 10.1039/C0SM01172J.
57. Appunni S, Rajesh MP, Prabhakar S. Nitrate decontamination through functionalized chitosan in brackish water. Carbohydr Polym. 2016 Aug 20;147:525-32. doi: 10.1016/j.carbpol.2016.03.075.